Chemical Engineering Science 268 (2023) 118446

Contents lists available at ScienceDirect

Chemical Engineering Science

journal homepage: www.elsevier.com/locate/ces

Effect of Wettability on Two-Phase Flow Through Granular Porous Media: Fluid Rupture and Mechanics of the Media

Mehryar Amir Hosseini [a], Serveh Kamrava [a], Muhammad Sahimi [b], Pejman Tahmasebi [a,*]

[a] Colorado School of Mines, Golden, CO 80401, USA
[b] Mork Family Department of Chemical Engineering and Materials Science, University of Southern California, Los Angeles, CA 90089-1211, USA

HIGHLIGHTS

- Fluid-particle interactions in multiphase fluid flow are considered.
- The effect of wettability on deformation is studied.
- Various fluid properties are considered to quantify how they change the fluid distributions and deformations.
- The results are compared with experimental studies and we found an excellent agreement.

ARTICLE INFO

Article history:
Received 18 April 2022
Received in revised form 9 December 2022
Accepted 1 January 2023
Available online 4 January 2023

Keywords:
Porous media
Multiphysics
Fluid flow, Discrete Element Method
Computational Modeling

ABSTRACT

A key parameter with considerable influence on the spatial distribution of the fluid phases in porous media is the wettability. Understanding the effect of wettability on fluids' distribution in three-dimensional (3D) porous media is critical to any phenomenon that involves multiphase flow in such media. To address the problem, we have carried out extensive computer simulations of two-phase flow in a 3D granular packing of grains and studied the effect of the wettability by varying the contact angle. To this end, the Immersed Boundary and Volume-of- Fluid approaches are coupled with the discrete element method (DEM). Five contact angles, covering a full range of wettability, are considered. We find that the wettability affects particle dynamics, such as the displacement of the grains, the contact force, and fluid velocity, and that rupture of the fluid can also occur in the pore space. Our results indicate that the volume of invading fluid injected into the system, the pressure on walls, and the injection surface decrease for larger contact angles. Most importantly, increasing the contact angle reduces the inter-particle interactions, whereas the drag force exhibits an opposite trend, leading to larger displacement of the particles. We also demonstrate and emphasize that some aspects of the effect of the wettability can only be observed in the 3D models of porous media and, thus, 2D models are inadequate.

1. Introduction

Multiphase fluid flow in porous media plays an important role in many natural phenomena and engineering processes (Sahimi, 2011; Blunt, 2017), including geological sequestration of CO_2 (Metz et al., 2005; Szulczewski et al., 2012), extraction of geothermal energy (Brown et al., 2012), water filtration (Cueto-Felgueroso and Juanes, 2008; Wang et al., 1978; Wei et al., 2014; Yao et al., 1971), hydraulic fracturing (Cueto-Felgueroso and Juanes, 2013; Lu et al., 2020; Patzek et al., 2013; Yuan et al., 2021; Zeng et al., 2016; Zhang et al., 2017), environmental cleanup (Avlonitis et al., 2003; Bartlett et al., 1995; Cao et al., 2020; Ebrahimi et al., 2010; Krzysztoforski et al., 2018; Maggay et al., 2021; Rajaei et al., 2021; Sarkar et al., 2012; Zheng et al., 2018), enhanced oil recovery, and many others. A wide range of physical factors influences spatial distribution of fluids in multiphase systems, such as permeability, wettability, mineralogy, ratio of viscosities and densities of the fluids, surface tension, flow rate, and morphological heterogeneity (Al-Raoush, 2009; Blunt et al., 2013; Cottin et al., 2010; Jiang et al., 2014; Lenormand et al., 1988; Nguyen et al., 2006; Rabbani et al., 2017; Yiotis et al., 2013; Zhang et al., 2011). Numerous experimental investigations have been carried out to understand the effect of the aforementioned properties on the flow characteristics (Osei-Bonsu et al., 2017; Reynolds and Krevor, 2015). Among such parameters, wettability has, however, received less attention due to the complexity of its interaction with the pore space.

* Corresponding author.
E-mail address: tahmasebi@mines.edu (P. Tahmasebi).

https://doi.org/10.1016/j.ces.2023.118446
0009-2509/

Wettability is defined as the fluid's tendency to cohere to a solid phase and is expressed in terms of the constant angle θ between the fluid and solid surface. When θ exceeds105°, the fluid is considered as nonwetting, whereas when θ < 65°, the fluid is referred to as wetting; for $65^\circ < \theta < 105^\circ$ one is in the *intermediate wettability* regime (Sahimi, 2011). The influence of the wettability is, therefore, conveyed through the interactions between the fluids and the solid surface of the pore space. As the result of the wettability properties of two fluids, two distinct displacement modes may be carried out, namely, drainage and imbibition. The former occurs when the displacing (invading) fluid is non-wetting, whereas in the latter case it is the wetting fluid that displaces the in-place (defending) fluid (Singh et al., 2019).

In some instances, wettability can trap fluid volume in pore spaces and/or influence the ruptured fluid's shape (Alhosani et al., 2021). In addition, occurrence of fluid rupture can have distinct outcomes. For example, in problems related to fluid recovery using another fluid, the fluid rupture must be minimized in order to achieve a higher recovery. In some engineering applications, such as CO_2 sequestration, however, it is desired to trap fluid in the pore space. Thus, due to its importance, fluid rupture has been widely studied, either through modeling, or experimentally (Golmohammadi et al., 2021; Shams et al., 2021).

A large number of experimental studies and computer simulations have been undertaken to study the effect of wettability in many multiphase flow problems in porous media (Bakhshian et al., 2021; Bradford et al., 1997; Heiba et al., 1983; Lin et al., 2021; O'Carroll et al., 2010; Yang et al., 2021; Zhao et al., 2018). Such studies demonstrated that wettability is a key factor whose effect cannot be neglected. The experiments can, however, be time-consuming, and the required setting is typically costly, especially when one studies the phenomenon in three-dimensional (3D) porous media (Zhang and Tahmasebi, 2022a,b;Zhang and Tahmasebi, 2018). The alternative is computer simulations, provided that an accurate model of the pore space and the relevant mechanisms of fluid flow and displacements are incorporated in the simulations. Nevertheless, most of the previous computer simulations that examined the impact of various wettability conditions were limited to 2D models (Davydzenka et al., 2020a,b; Meng et al., 2020; Nhunduru et al., 2022; Zhou et al., 2022). Many factors contribute to the difficulty of studying the effect of wettability in 3D media. In particular, experimental visualization of the effect of wettability is complex. Computer simulation of any multiphase flow problem in 3D porous media is also complex, at least compared with the corresponding 2D modeling. A summary of recent studies of the effect of wettability on fluid flow is given in Table 3.

The goal of the present paper is to report on the results of a comprehensive study of the effect of wettability on fluid flow in 3D media for a wide range of contact angles ($30^\circ \leqslant \theta \leqslant 150^\circ$). We simulate flow of two immiscible fluids – the displacing and displaced, or the invading and defending, fluids – at pore scale in a granular porous medium. As described below, our approach to computer simulation is capable of capturing fluid–fluid, particle–particle, and fluid-particle interactions and, hence, represents a comprehensive model that provides important insights into the effect of the wettability on the phenomenon that we study.

A number of approaches to simulating two-phase flow in porous media has already been developed. Aside from pore-network models that have been the standard approach for the problem since the 1980 s (Blunt, 2017; Sahimi, 2011), one approach is based on the Eulerian-Eulerian coupling of fluid and solid phases (Baker et al., 2020; Chiesa et al., 2005; Kalteh et al., 2011; le Lee and Lim, 2017; Duarte et al., 2009; Patel et al., 2017; Peng et al., 2020; Pilou et al., 2011; Swain and Mohanty, 2013; Zhang et al., 2019). The approach considers, however, both fluids and solid phases as continuous, and while it might be a suitable method for large-scale systems, it cannot be used in a pore-scale study. Smoothed particle hydrodynamics is another numerical method that has been used for simulating multiphase flow systems (el Shamy and Sizkow, 2021; He et al., 2018b; Peng et al., 2021; Tang et al., 2018; Xu et al., 2019), but its capability for accurate computation and study of fluid–fluid interface at pore scale has not, to our knowledge, been demonstrated. Lattice Boltzmann (LB) model (Aljasmi and Sahimi, 2021; Han and Cundall, 2013; Kohanpur et al., 2020; Xiong et al., 2014; Yang et al., 2018) can also be used for simulating modeling of two-phase flow in 3D porous media, although the LB method can be used for studying the wettability effect only through parametrization of the algorithm whose physical justification is not entirely established. In addition, it should be pointed out that these methods cannot account for the behavior of particles in a granular medium. Despite their accuracy in simulating particle-scale systems, the Lagrangian approaches, such as the Discrete Element Method (DEM), cannot also take directly into account the presence of fluids.

Thus, to simultaneously capture the behavior of fluid–fluid and fluid-particle interactions in a porous medium, the Eulerian-Lagrangian coupling approach (EL) was proposed in which the Eulerian formulation is used for calculating fluid–fluid interfacial properties, while the Lagrangian approach considers each particle as an object whose effect is taken into account. In the present paper, we utilize an EL approach coupled with a computational fluid dynamics (CFD) technique, the volume of fluid (VOF) approach, which has been demonstrated to be capable of tracking the fluid–fluid interface with significant accuracy (Ge et al., 2020; Issakhov and Imanberdiyeva, 2020; Issakhov and Zhandaulet, 2020; Pozzetti and Peters, 2018).

A well-known EL coupling method is the CFD-DEM (Golshan et al., 2020; He et al., 2018a; Kuang et al., 2020; Li and Zhao, 2018; Lungu et al., 2021; Mao et al., 2020; Wang et al., 2019a; Wang et al., 2020) in which the CFD and DEM simulate, respectively, the fluid and solid phases. The Navier-Stokes equations, or the Stokes' equation for slow fluid flow, are solved to simulate the fluid flow and the interaction between the fluid phases, while and the trajectory of each particle is simulated based on Newton's second law of motion, incorporated in the DEM. Depending on the resolution of the fluid domain, the CFD-DEM coupling may be divided into two distinct approaches (Norouzi et al., 2016): (i) unresolvedor coarse-scale simulation (Bérard et al., 2020; Blais et al., 2016; Golshan et al., 2020; He et al., 2022; Kuruneru et al., 2019; Vångö et al., 2018; Yao et al., 2020) and (ii) resolved computations (Kloss et al., 2012; Nguyen et al., 2021a,b; Wang et al., 2019b; Hager et al., 2014; Wang and Liu, 2020). The former utilizes a computational grid with grid blocks much larger than the size of the particles, whereas the latter demands the opposite. Thus, the unresolved approach allows one to simulate large-scale systems, whereas the resolved methods can simulate small systems, but have higher accuracy than the unresolved approach and reveal much fine-scale information.

In the present paper, we use the resolved CFD-DEM approach, as our goal is to capture the pore-scale behavior of the fluids-particle interactions in a multiphase flow system. In addition, previous investigations showed that the VOF method is capable of modeling such complex multifluid systems (Ge et al., 2020; Issakhov and Imanberdiyeva, 2020; Issakhov and Zhandaulet, 2020; Pozzetti and Peters, 2018). Hence, the resolved VOF-DEM coupling approach can be fruitfully utilized to capture the fluid–fluid and fluid-particle interactions in a 3D pore space. As described below, we combine the immersed-boundary (IB) method (Peskin, 1977) with the VOF approach and develop the multifluid IB-VOF coupling to investigate the influence of a variety of wettability conditions on fluids' motion and their effect on grains in porous media and granular materials.

The rest of this paper proceeds as follows. In *Sec.* 2, the governing equations for the DEM, the CFD, and the IB-VOF coupling that we develop are described. The simulation system and the boundary conditions will be explained in detail in *Sec.* 3. The results will be presented and discussed in *Sec.* 4. The last section summarizes the paper and draws the conclusions of the study.

2. Computer simulation

In this section, the essential elements of our computer simulations are described. The computations involving coupling of fluids and grains consist of three parts, namely, the CFD and DEM, and how the two are coupled. The DEM is used to account for the inter-particle forces, after which the general concept of the VOF method and its formulations is presented. The coupling of the two will then be described.

2.1. Discrete element method

The DEM was originally proposed (Cundall and Strack, 1979) for simulating granular media. Each particle has translational and/or rotational motion. The approach allows exchange of momentum and energy between the particles whenever a collision occurs between them. Two types of forces acting on particles are accounted for, namely, contact, and non-contact forces. In the present paper, however, we consider only the contact forces, since non-contact forces can be neglected in the type of porous media that we consider. Newton's equations of motion for particle$i$ of mass m_i,

$$m_i \frac{d v_i}{dt} = \sum_j f_{ij}^c + f_{ij}^{fp} + f_i^g, \tag{1}$$

takes into account its transitional motion with velocity v_i, to which a contact force f_{ij}^c is applied, when particles i and j are in contact. The effect of the presence of the fluids, as well as that of gravity, is considered through the fluid-particle force f_{ij}^{fp} and gravitational forcef_i^g.The rotational motion of particle$i$, when it has a collision with particle$j$, is represented by,

$$I_i \frac{d\omega_i}{dt} = \sum_j T_{ij}. \tag{2}$$

in which I_i and ω_i are rotational inertia and velocity, respectively, and T_{ij} is the torque acting on particle$i$, due to its collision with either wall boundaries or particle$j$:

To calculate the contact forces f_{ij}^c between two particles, we use the non-linear Hertzian contact model, which includes the Young's modulus and Poisson's ratio of the particles (Bakhshian and Sahimi, 2016; di Renzo and Paolo Di Maio, 2005). The fluid-particle interactions force f_{ij}^{fp} will be described below.

2.2. The governing equations for volume of fluid method

We used the VOF method to simulate the two-phase fluid flow, which has been utilized by many in the past in the simulation of multiphase fluid systems in order to capture accurately the interface between the fluids. The method solves the advection equation *for a mixture of fluids* in order the evaluate the interface between fluids. Considering the presence of the solid phase, i.e., the grains, the equation to solve is given by

$$\frac{\partial \beta \varepsilon_i}{\partial t} + \nabla.(\beta \varepsilon_i \boldsymbol{v}_f) = 0, \tag{3}$$

where β is solid void fraction, ε_i is the volume fraction of the fluid$i$, and $\boldsymbol{v}_f$ is fluid velocity. After adding the *interface compression* term to Eq. (3), the equation is extended to,

$$\frac{\partial \beta \varepsilon_i}{\partial t} + \nabla.(\beta \varepsilon_i \boldsymbol{v}_f) - \nabla.(\boldsymbol{v_r} \varepsilon_i (1-\varepsilon_i)) = 0, \tag{4}$$

where $\boldsymbol{v_r}$ is the relative velocity, i.e., the difference between the velocities of the liquid and air. To solve the momentum and continuity equation for a mixture of fluids, the volume-weighted fluid-mixture properties are used, which for a two-phase flow system, are given by

$$\rho_f = \varepsilon_i \rho_i + \varepsilon_j \rho_j, \tag{5}$$

$$\mu_f = \varepsilon_i \mu_i + \varepsilon_j \mu_j, \tag{6}$$

where ρ_i denotes the density of fluid$i$, and μ_i is the viscosity of fluid$i$. Let us point out that since the resolved CFD-DEM method is used in this paper, the volume fraction ε for both fluids can be zero, if a cell is completely filled by the solid phase. Since we study a fluids-particle system, the Navier-Stokes equations should be modified to account for the presence of the solid phase. The momentum equation is, therefore, rewritten in the following form,

$$\begin{aligned} \rho_f \frac{\partial \beta v_f}{\partial t} + \nabla.\left(\beta \rho_f v_f v_f\right) &= -\beta \nabla\left(p - \rho_f g.x\right) \\ &+ \beta \nabla.\left(\mu_f\left(\nabla v_f + \nabla v_f^T\right) - \frac{2}{3}\mu_f I \nabla.v_f\right) \\ &- \int \in g.\nabla \rho_f + \beta F^{SF} + F^{drag}. \end{aligned} \tag{8}$$

Here, $\boldsymbol{F}^{fp}$ is the fluid-particle interaction force, $\boldsymbol{g}$ is the gravitational acceleration, x is the position vector, $\boldsymbol{I}$ is the identity tensor, and $\boldsymbol{F}^{SF}$ denotes surface tension. The equation for the surface tension should also be modified in order to account for the two fluids (see also Fig. 1),

$$F^{SF} = \sum_{ij} \sigma_{ij} k_{ij} (\varepsilon_j \nabla \varepsilon_i - \varepsilon_i \nabla \varepsilon_j), \tag{9}$$

where σ is the surface tension, and the interface curvature k for two fluids i and j is given by

$$k_{ij} = \nabla.\hat{n}_{ij}. \tag{10}$$

$$\hat{n}_{ij} = -\frac{\left(\varepsilon_j \nabla \varepsilon_i - \varepsilon_i \nabla \varepsilon_j\right)}{\left|\varepsilon_j \nabla \varepsilon_i - \varepsilon_i \nabla \varepsilon_j\right|} \tag{11}$$

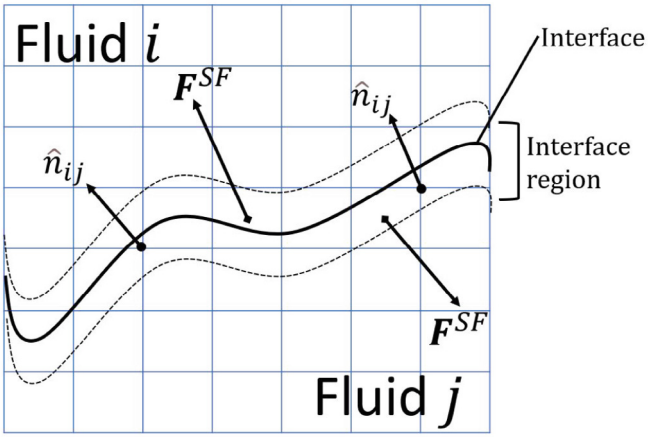

Fig. 1. Illustration of normal vector $\hat{\boldsymbol{n}}_{ij}$ and surface force $\boldsymbol{F}^{SF}$ between fluid i and j at the interface region.

2.3. Resolved CFD-DEM coupling

Computationally, the resolved CFD-DEM coupling differentiates between grid blocks occupied by the fluids, particles, or both, in order to attain high accuracy in the simulations, which, as discussed in the Introduction, is needed for the pore-scale problem that we study. In our computations, the linear size of each block or call was 1/10 of the particles' diameter. To have the required high accuracy and resolution, the size of the grid blocks used in the CFD computations much be smaller than particle size. Thus, the fluid's velocity field should be corrected in the blocks, which are partially or fully occupied by the particles. To reach the desired resolved CFD-DEM coupling, the following steps are taken,

(1) The fluids and particles are initialized by their initial volume fractions, boundary conditions, and particles' locations.
(2) The CFD solver computes the velocity and pressure fields with a pressure-implicit split operator (PISO) method (Issa, 1986). The presence of a solid phase is neglected in this step.
(3) The particles' positions and velocities are calculated by the DEM solver, after which the result is passed to the CFD part of the coupling.
(4) Based on the DEM results, the CFD cells that are completely or partially occupied by the particles are identified.
(5) The volume fraction of all fluid cells is determined, and fluid cell conditions are updated by the continuity equation, Eq. (7).
(6) The velocity and pressure fields of fluids, which were computed in step 2, are corrected based on the particles' velocities. In order to do that, first, the calculated velocity in step 2 - v_f from Eq. (8) - should be updated based on the particle's velocity to construct a new velocity field v_f^c. To utilize the new velocity field in the Navier-Stokes equations, F_C in Eq. (12) should be added to the right side of Eq. (8); that is,

$$F_C = \rho_f \frac{\partial}{\partial t}\left(v_f^c - v_f\right). \tag{12}$$

Then, to solve the divergence-free equations, v_f^c, v_f' is represented by

$$v_f' = v_f^c - \nabla . v_f^c \tag{13}$$

Furthermore, a correction term, $\frac{\partial\left(\nabla . v_f^c\right)}{\partial t}$, should be added to the pressure term in Eq. (8). Therefore, Eq. (8) is modified to

$$\begin{aligned}\rho_f \frac{\partial \beta v_f'}{\partial t} + \nabla.\left(\beta \rho_f v_f v_f\right) = &-\beta\left(\nabla p - \nabla \rho_f g.x + \rho_f \frac{\partial \nabla . v_f^c}{\partial t}\right) \\ &+ \beta\nabla.\left(\mu_f\left(\nabla v_f + \nabla v_f^T\right) - \frac{2}{3}\mu_f I \nabla . v_f\right) \\ &- \int g.x\nabla\rho_f + \beta F^{SF} + F^{drag} + F_C,\end{aligned} \tag{14}$$

(7) The new velocity and pressure fields are transferred to the DEM part to apply to the particles.
(8) The algorithm is repeated from step 1 until it reaches the final timestep.

3. Model of granular porous media

To examine the effect of the wettability in 3D porous media and capture pore-scale behaviors, a cylindrical domain with a radius of 13.25 mm and height of 30 mm was used, which is based on a previous 2D study (Meng et al., 2020). The simulated domain is shown in Fig. 2(a). To generate a packing of grains, particles with a diameter of 2 mm were inserted by a separate DEM simulation and were allowed to reach the equilibrium state by the gravitational force. The result was a packing of 1,948 particles. The CFD-DEM coupling was started after all the initial particles' force, velocity, and displacement were set to zero. The generated packing had a porosity of 51 %, with the final structure shown in Fig. 2(b).

Furthermore, the CFD domain was initially saturated with the defending fluid. The density and viscosity of the defending fluid phase were taken from a previous study (Al-Awadi, 2011). Water was injected as invading phase from a plane at the bottom of the domain with a constant rate. The contact angles were varied between 30° and 150° in order to investigate the wettability effects on the morphology and flow properties of the pore-scale system. The properties of the particles and fluids listed in Table 1 and Table 2, respectively. The injection plane was used as an inlet;

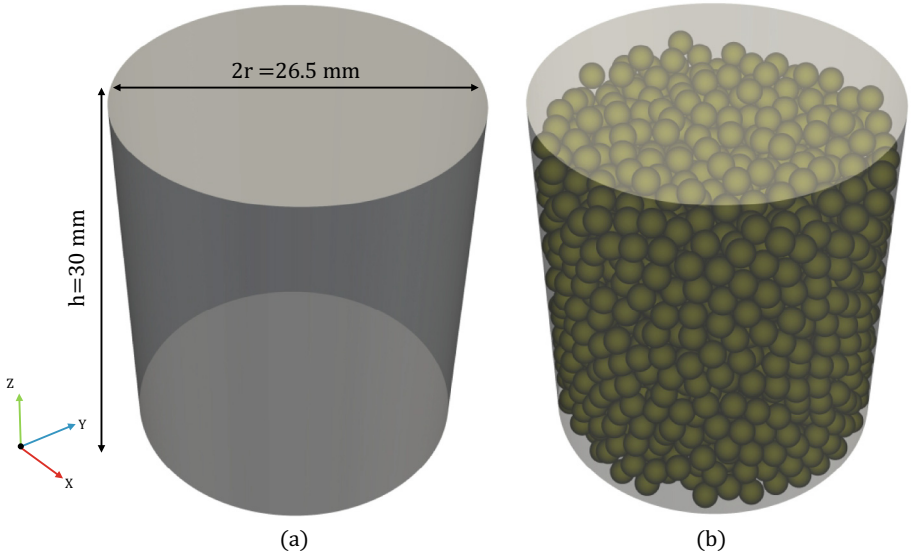

Fig. 2. (a) The shape and dimensions of the model, and (b) the final packing of particles used in the computations.

Table 1
Properties of particles used in the simulations.

Property	Value
Young's modulus (Pa)	5×10^6
Poisson's ratio	0.4
Friction Coefficient	0.5
Restitution Coefficient	0.3
Density of Particle (kg/m^3)	2500
Diameter (m)	0.002

Table 2
Properties of fluids used in the simulations.

Property	Value
Density of invading fluid (kg/m^3)	1000
Density of defending fluid (kg/m^3)	920
Kinematic viscosity of invading fluid (m^2/s)	1×10^{-6}
Kinematic viscosity of defending fluid (m^2/s)	4.13×10^{-3}
Surface Tension (kg/s^2)	0.013
Contact Angles (°)	[30°, 60°, 90°, 120°, 150°]
(log) Capillary number	−0.48

no-slip boundary condition was used on the walls, and a pressure was applied at the outlet on the top plane. We used the drag force model suggested by Shirgaonkar et al. (2009) in the resolved CFD-DEM coupling simulations. The timestep for both CFD and DEM was 10^{-6} s; hence, the coupling time step ratio, the ratio of the DEM time step to CFD time step, was 1.

4. Results and discussion

To validate the model, as well as the results of the computer simulations, we compare the results with 3D experimental studies. To do so, injection pressure will be compared to previous experimental studies (Zhao et al., 2016). After demonstrating the accuracy of the method, the effect of wettability on fluids characteristics and the behavior of the particles will be quantified using injection pressure, wall pressure, drag and inter-particle forces, particle velocity, and the packing displacement. To comprehensively study the impact of the various wettability conditions, the parameters in Table 1 and Table 2, except for the contact angle, were kept constant in the simulations. The injection pattern of the invading fluid during the simulation for $\theta = 30^\circ$ and the invading fluid rupture are shown in Fig. 3. As can be seen, the invading fluid is well distributed in the domain, and the effect of the presence of compact packing of particles is also clearly evident in Fig. 3.

Fluid rupture is developed during simulations, one of which is shown in Fig. 3(h). The influence of the contact angle on the formation of ruptures near the solid phase is illustrated in Fig. 4, where the particles and fluid phases around one point of rupture are shown in more detail in Fig. 4(a). Furthermore, visually inspecting the results, the invading fluid and two grains that shaped its distribution around them are clearly seen in Fig. 4(b).

Hence, to gain deeper understanding of the effect of the wettability on the rupture phenomenon, the patterns of the invading fluid phase for various contact angles are shown in Fig. 4(c) - (e). The results imply that with increasing contact angle, the volume of the invading fluid near the particles decreases. As a result, for the lowest contact angle that we considered, i.e.,$\theta = 30^\circ$, a larger fraction of the particles' surface is wetted by the invading phase, which are in line with the definition of the contact angle.

Extensive simulations were carried out over a wide range of contact angles, as listed in Table 2. The distribution of the invading fluid for various wettability conditions at the bottom plane (at Z = 0.0 mm) and close to the bottom plane (at Z = 0.2 mm) are shown in Fig. 5(a) and Fig. 5*(b)*, respectively, while the droplet formation corresponding to the contact angles is presented in Fig. 5(c). In general, narrow channels and more ruptures in the invading fluid are seen at lower contact angles, which establish the impact of wettability on fluid's characteristics.

We analyzed the images shown in Fig. 5(a) and 5(b) in order to determine the fraction of the particles' surface covered by the invading fluid. Two distinct behaviors were discerned in the selected plates. As illustrated in Fig. 5(a), which is quantified in Fig. 5(d), at the bottom wall at Z = 0.0 mm, the area of the invading fluid decreases with increasing contact angles. Near the wall plate at Z = 0.2 mm, however, the trend is the opposite of what is shown in Fig. 5(a). As shown in Fig. 5(c) and marked in Fig. 4, for lower contact angles, a larger area of the solid phase (e.g., the walls) is in contact with the invading fluid, which is, of course, expected. Nevertheless, the behavior of the fluid near the bottom plate is not identical to those at higher levels. This contradiction in the behavior of invading fluid on the bottom wall and close to it highlights the imperativeness of 3D simulations for understanding the effect of wettability, since this effect is absent in 2D systems.

Simulation in 3D models of porous media allows analyzing and comparing the volume (or saturation) of the invading and defend-

Table 3
Summary of the recent studies of the effect of wettability on fluid flow.

Reference	Approach	Detail
(Nhunduru et al., 2022)	Numerical	The effect of wettability was studied in pore-scale using VOF.
(Zhou et al., 2022)	Numerical	2D LBM was applied to examine the impact of the wettability and Capillary on fluid displacement and saturation.
(Yang et al., 2021)	Numerical	The impact of wettability and Capillary number on remaining oil distribution using the VOF method.
(Bakhshian et al., 2021)	Numerical/ Analytical	LBM simulations to study the effect of different wettability and mobility conditions on saturation, displacement pattern, and the Euler characteristic density of the defending fluid.
(Lin et al., 2021)	Numerical	Estimate the recovery degree of tight sandstone under different contact angles with LBM.
(Davydzenka et al., 2020a)	Numerical	Applying Unresolved CFD-DEM to study the effect of wettability on fluid velocity, Drag force, and void fraction in different Capillary numbers.
(Davydzenka et al., 2020b)	Numerical	Deploying Resolved CFD-DEM to study wettability's influence on velocity, Drag force, and displacement.
(Meng et al., 2020)	Numerical	Two-phase flow and DEM to study the injection pressure, shear stress, and particle stress.
(Li et al., 2019)	Experimental	Examine the effect of the surface wettability of a spherical particle on the behavior of the flow.
Zhao et al., 2018	Numerical	Effect of Wettability on relative permeability with Lattice Boltzmann Method (LBM).
(AlRatrout et al., 2018)	Experimental	Relation between wettability and surface roughness.
(Zhao et al., 2016)	Experimental	Wettability effects in different Capillary numbers.
(Holtzman, 2016)	Numerical/ Experimental	The influence of pore-disorder on fluid dislocation in drainage and imbibition conditions.

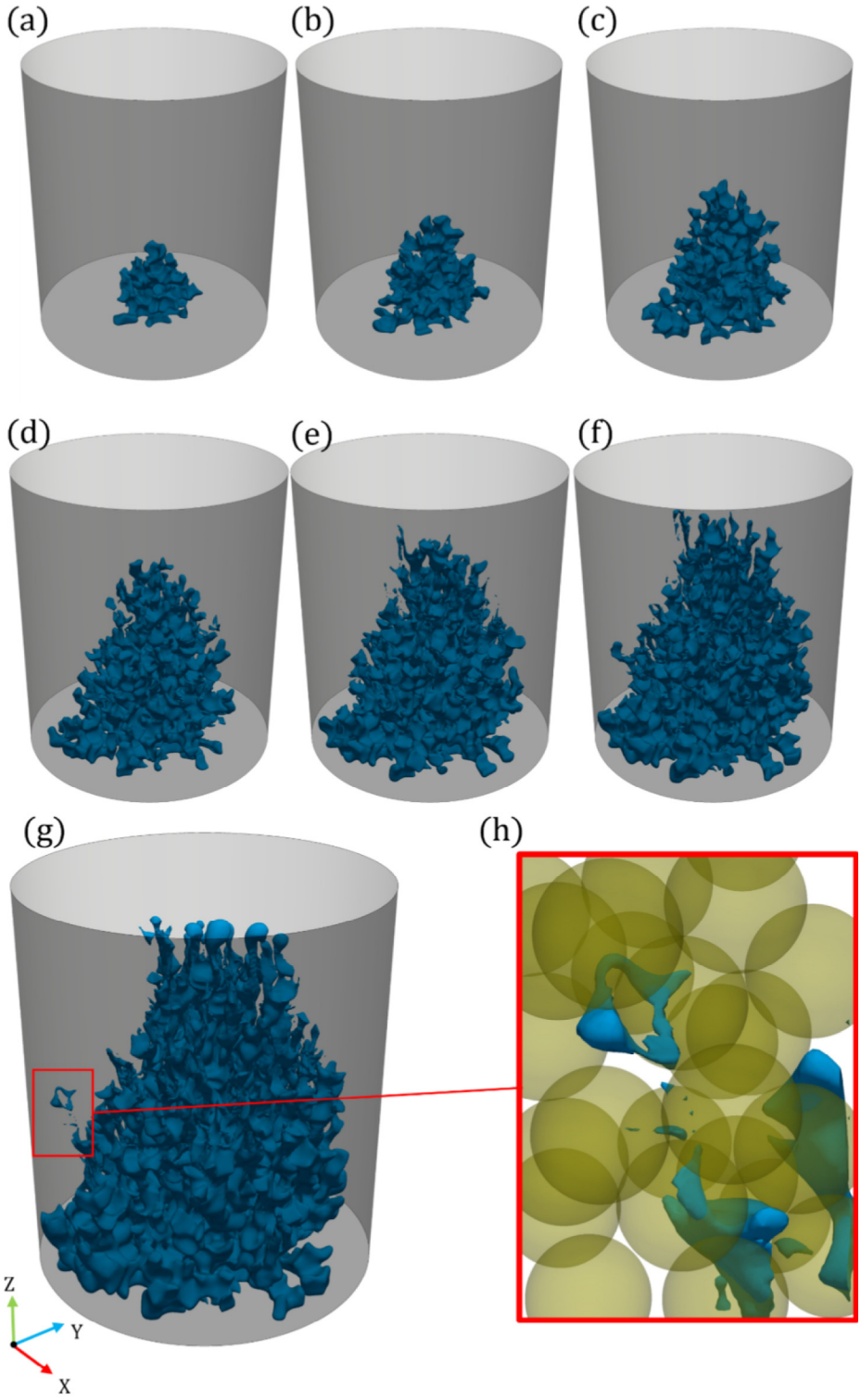

Fig. 3. Dynamic evolution of the invading fluid at (a) 0.05 T; (b) 0.1 T; (c) 0.2 T; (d) 0.4 T; (e) 0.8 T, and (g) T, where T is the total simulated time. (h) A close snapshot of fluids-particle interactions near particles when rupture happened in the invading fluid for$\theta = 30^{\circ}$.

ing fluids and their dependence on the contact angle in a physically meaningful manner, whereas the corresponding simulation in 2D models of pore space does not allow such a comparison. Moreover, due to the percolation effect (Sahimi, 2023) simultaneous formation of sample-spanning clusters of *both* fluids in a 2D model of porous media is impossible. Although in our simulations the injection rate was kept a constant for all the contact angles, we observe pore-scale differences in the distribution of the invading fluid, as shown in Fig. 4, implying that the volume of invading fluid at the same time step for various contact angles should be analyzed. This is shown in Fig. 6. As can be seen, the volume of invading fluid decreases in the domain with increasing contact angle, implying

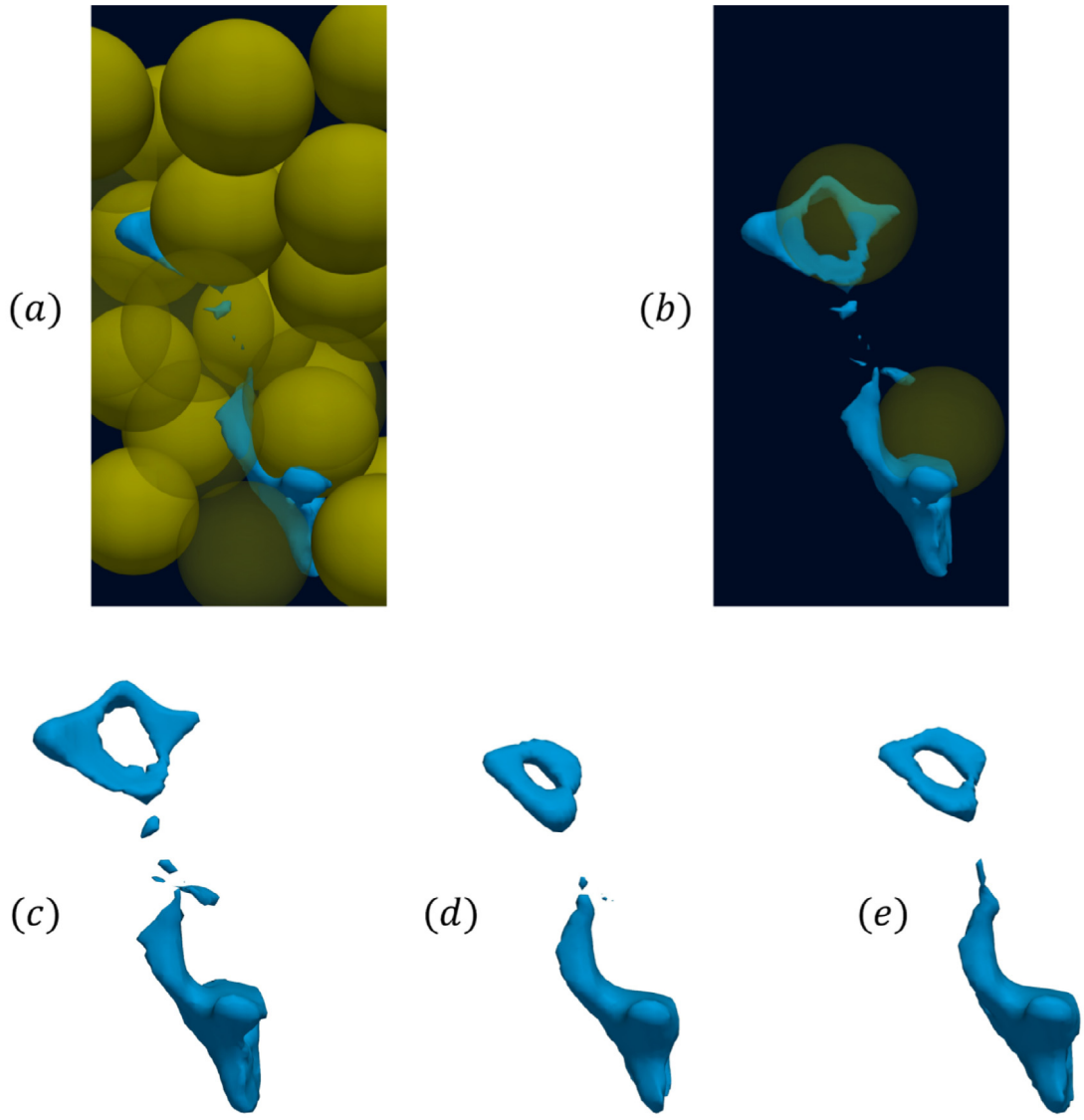

Fig. 4. Demonstration of (a) fluid rupture as a result of the interaction of the packing of particles with the invading and defending fluids for$\theta = 30^{\circ}$; (b) configuration of the invading fluid, and invading fluid's shape for (c) $\theta = 30^{\circ}$ (imbibition), (d) $\theta = 90^{\circ}$ (intermediate wettability), and (e) $\theta = 150^{\circ}$ (drainage).

that, compared to intermediate wettability and drainage during imbibition corresponding to low contact angle, the invading fluid is more efficiently distributed in the pore space,. This is in agreement with the proposal of Cieplak and Robins (1990) that during imbibition the displacement pattern is compact, whereas during drainage it forms a fractal structure (Yang et al., 2021).

Two other important quantities are the injection pressure and the pressure (or stress) that the fluid exerts on the wall of the cylindrical porous medium, and their dependence on the contact angle. Fig. 7 presents the computed pressures and their dependence on the contact angle. It indicates that, over short time scales, the contact angle has no discernable effect on the injection pressure. But, over longer time scales, notable differences emerge and, more importantly, the injection pressure for strong drainage,$\theta = 150$, tends to decrease more than those for intermediate wettability and imbibition. These results are in qualitative agreement with the experimental data (Zhao et al., 2016). According to Fig. 7(b), similar trends also develop for the contact angle-dependence of the pressure at the wall, such effect is a bit stronger, especially at shorter times.

Another way of differentiating between the various wettability conditions is through the average drag force that the fluids exerts on the grains. The drag force was computed by two methods. One was the drag force $< F_d >$ averaged over all the contact angles and all the grains. The second drag force was an average over all the particles, but computed for the individual contact angles, which was then normalized by its value at$\theta = 90^{\circ}$, in the middle of contact angle range, which we refer to as "neutral" wettability. The results are presented in Fig. 8(a) and Fig. 8(b), respectively.

Before starting the injection at time$t = 0$, the drag force is zero. After a single timestep, the drag force takes on its highest value, due to injection of the invading fluid into the domain at a constant rate. Afterward, the drag force decreases as time passes, since the invading fluid forces its way into the 3D domain, with trends that are similar to those of the injection and wall pressures, shown in Fig. 7. On the other hand, the dynamic evolution of the normalized drag force for each contact angle, shown in Fig. 8(b), implies that for lower contact angles ($\theta < 90^{\circ}$) the drag force is higher than the "neutral" condition at $\theta = 90^{\circ}$, which also is in agreement with the behavior of the pressure for various contact angles. As the con-

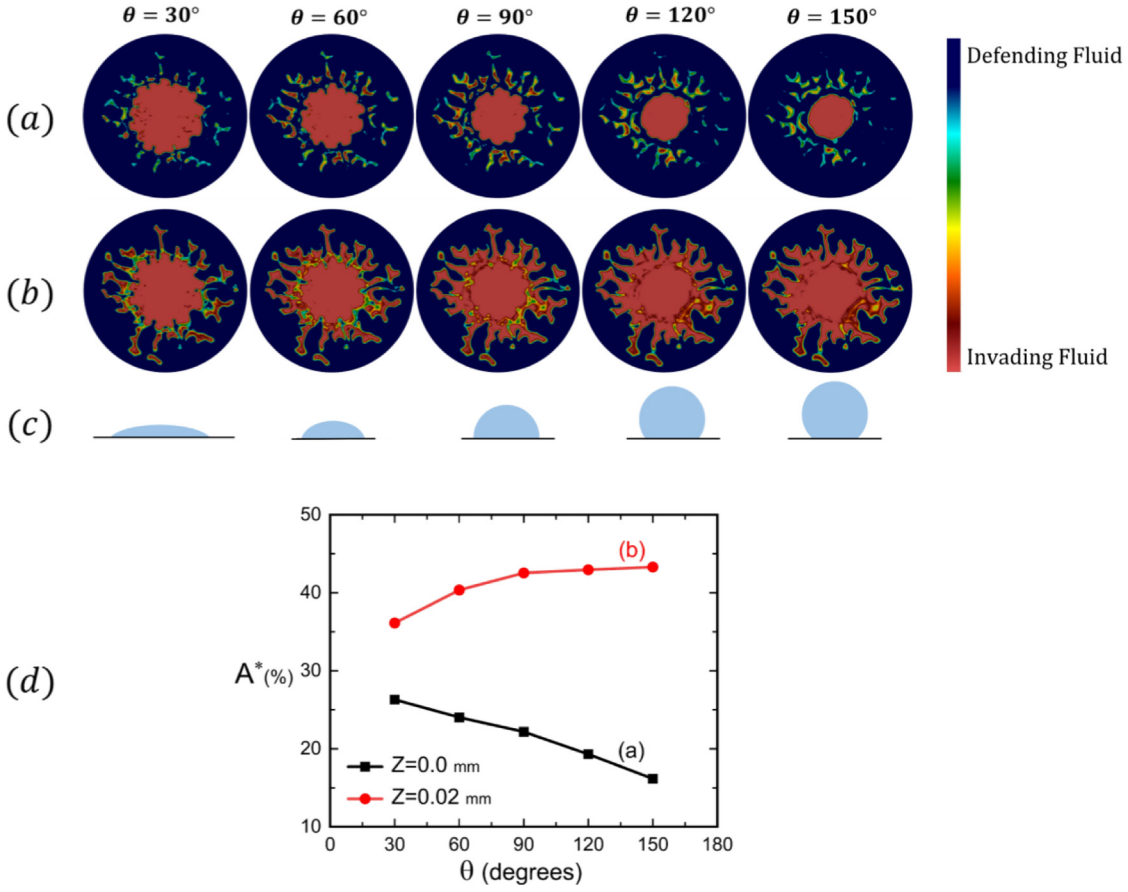

Fig. 5. The effect of contact angle, at the same time step, at axial positions (a) Z = 0.0 mm, and (b) Z = 0.2 mm. (c) The effect of contact angle on the shape of a droplet near the wall. (d) The ratio of the area of invading and that of the total surface A^* that quantifies the behavior of the invading fluid at the bottom wall (i.e., Z = 0.0 mm) and close to it (i.e., Z = 0.2 mm).

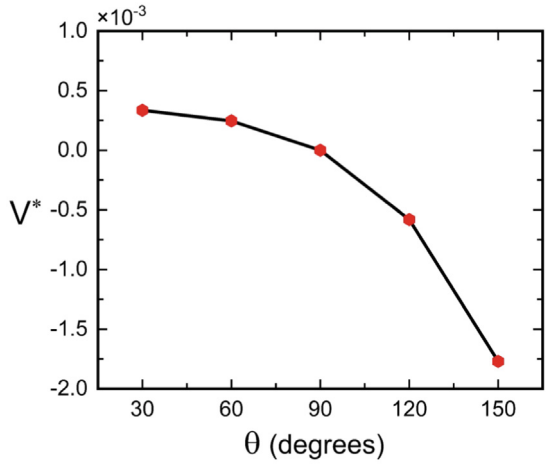

Fig. 6. Dependence of the normalized volume of invading fluid V_* $(= \frac{V_{\theta-} - V_{\theta=90^\circ}}{V_{\theta=90^\circ}})$, at the end of the simulations, on contact angleθ.

tact angle increases the drag force exerted on the particles decreases, such that it is the lowest under strong drainage conditions,$\theta > 90^\circ$, which is expected.

Another quantity of great interest is the average inter-particle force F_p. Similar to the drag force, we computed an average inter-particle force $< F_p >$, with the averaging taken over all the contact angles and all the grains, and also the average inter-particle forces for each contact angle, averaged over the particles and normalized the results by the value for neutral wettability for $\theta = 90^\circ$. The results are presented in Fig. 9. Since, as pointed out earlier, the flow simulation and its coupling with the granular medium began after the medium had reached its equilibrium state, the inter-particle force is initially zero. After the initial time step, however, collisions between the particles are caused by the injection of the invading fluid into the domain and the gravitational force, which generate the inter-particle force with its value increasing sharply. The sharp increase in F_p is more pronounced than the corresponding drag force, since nearly 2,000 particles begin to move and collide at microscale. At the end of the simulation, on the other hand, the particle–particle force is nearly zero, whereas there is still a residual drag force, as shown in Fig. 8(a). The reason for this behavior is the damping that is applied in the DEM calculations. Most of the drag force is, therefore, damped by collisions at the end of the simulations since it is not strong enough to overcome the damping.

Fig. 9(b) depicts the influence of the contact angle on the inter-particle force. The results indicate that the inter-particle force increases with increasing contact angle, achieving its maximum at $\theta = 90^\circ$. The direct relation between the inter-particle force and wettability is striking, as one would expect intuitively that the force should not depend on the contact angle. This is also in contrast with the behavior of the drag force and pressure. This may be explained based on the nature of the contact angle, since when the angle is low, more area of the particles is in contact with the fluid phase. Thus, increasing the area of the fluid on the surface of a particle decreases the possibility of collision between two particles since a particle is in more contact with the fluid phase than with another particle.

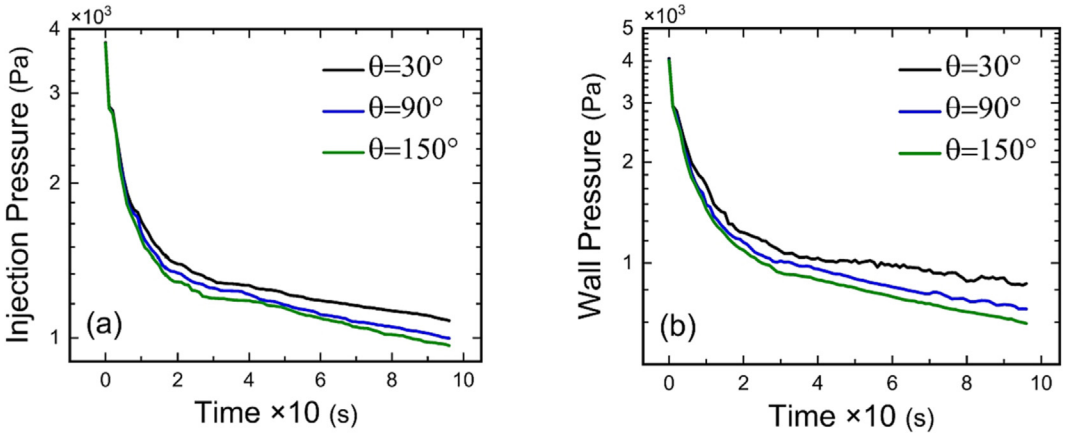

Fig. 7. Comparison of the dynamic evolution of (a) injection pressure, and (b) pressure at the wall for imbibition,$\theta = 30^{\circ}$, intermediate or neutral wettability,$\theta = 90^{\circ}$, and drainage,$\theta = 150^{\circ}$.

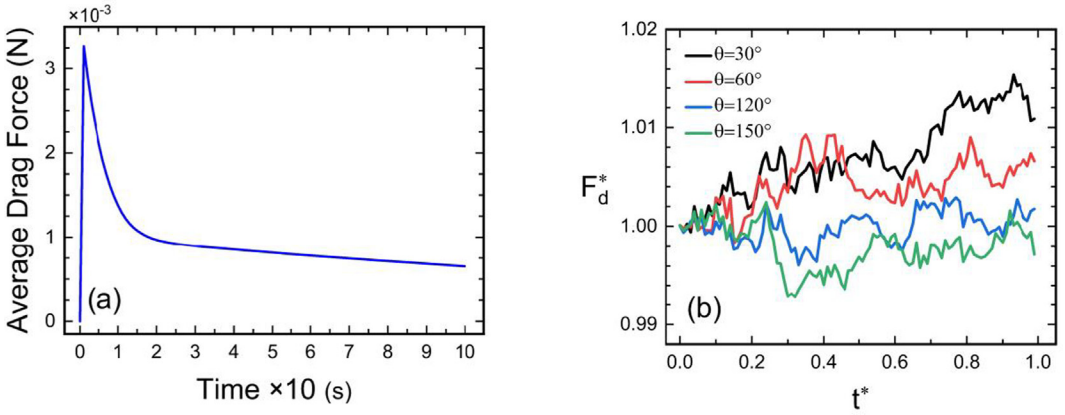

Fig. 8. Dynamic evolution of (a) the average drag Fd force for all the contact angles, and (b) the individual drag forces Fd * for each angle, normalized by its value at$\theta = 90^{\circ}$. t* is the dimensionless time by dividing the actual time by the total time that was simulated.

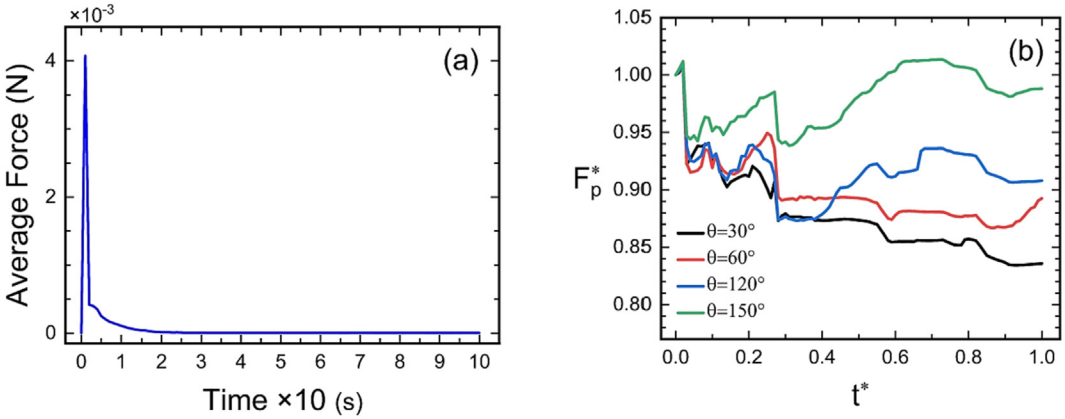

Fig. 9. The evolution of (a) average inter-particle force for all the contact angles, and (b) the normalized inter-particle force for several contact angles. t*is the dimensionless time by dividing the actual time by the total time that was simulated.

The effect of the fluid phase on the velocity of particles is also interesting and physically important. Thus, we also computed two particle velocities and studied their dynamic evolution. One, <*v*>, represents the average velocity for all the wettability conditions, the results for which are shown in Fig. 10(a). The second computed velocity was that of the particles, normalized by the neutral wettability conditions at$\theta = 90^{\circ}$; see Fig. 10(b). The general trends of the average velocity are consistent with those of the injection pressure, shown in Fig. 7(a), wall pressure in Fig. 7(b), drag force in Fig. 8(a), and particle–particle force in Fig. 9(a). The velocity of the particles is, of course, initially zero, but after the invading fluid is injected into the pore space, it rises sharply. Thereafter, with the propagation of the invading fluid in the pore space, the particles' velocity experiences a gradual fall. To further

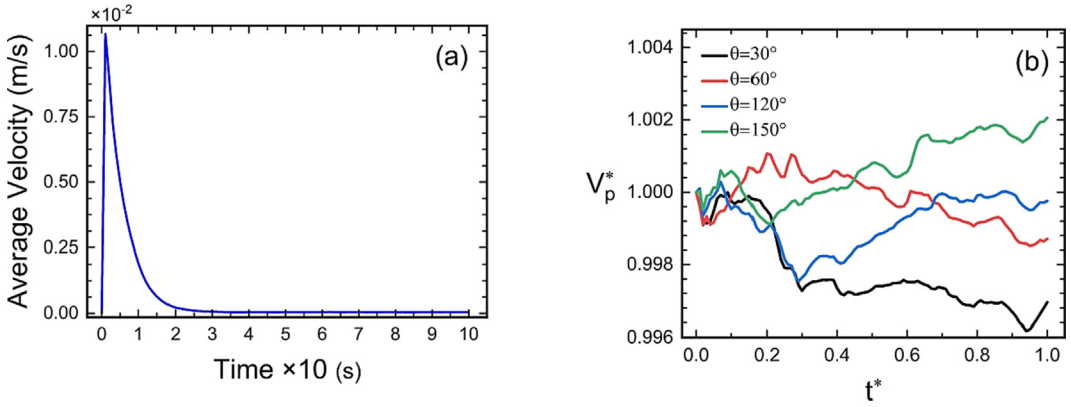

Fig. 10. The evolution of (a) average particles velocity for all the contact angles, and (b) the normalized velocity of particles for several contact angles. t* is the dimensionless time by dividing the actual time by the total time that was simulated.

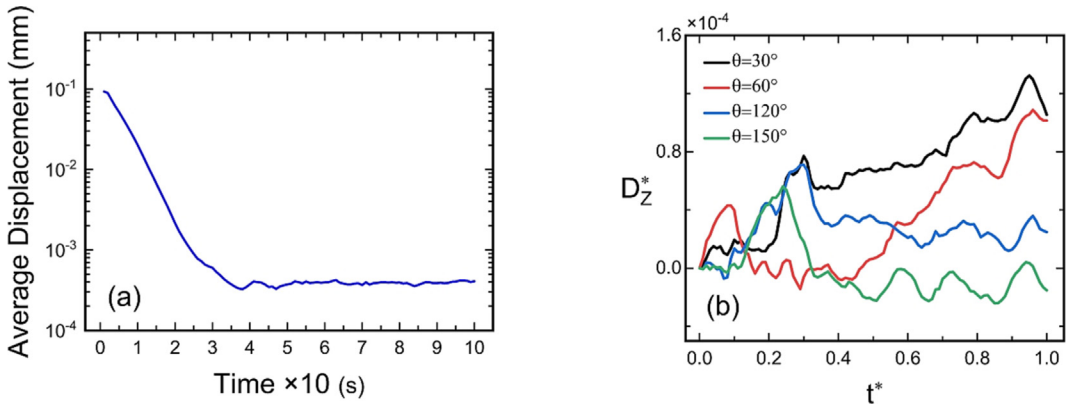

Fig. 11. The evolution of (a) average particle displacement in the axial Z-direction for all the contact angles and (b) the normalized Z- displacement for several contact angles. t* is the dimensionless time by dividing the actual time by the total time that was simulated.

evaluate the effect of the wettability on the particle velocity, its evolution for each contact angle, normalized by its value at$\theta = 90^{\circ}$, is shown in Fig. 10(b). In the limit of long times, the velocity of the particles during imbibition ($\theta = 30^{\circ}$) and drainage ($\theta = 150^{\circ}$) have, respectively, the lowest and highest values. The results also point to the importance of the inter-particle force in such systems.

Finally, dependence of the displacement u_p of the particles on the contact angle was studied. Intuitively, one expects the displacements to occur mostly in the axial *Z*-direction, and the simulations do confirm this Thus, once again, we computed the average displacement $< u_p >$, with the average taken over all the contact angle, as well as the dynamic evolution of the particle displacement for each contact angle, normalized by their value at$\theta = 90^{\circ}$; see Fig. 11. The qualitative features of the results are similar to those of drag and inter-particle forces, as well as the average particle velocity, namely, the average *Z*-direction particle displacement for all the wettability experiences the highest values, after which it decreases with time; see Fig. 11(a) and 11(b).

5. Summary and conclusions

The primary purpose of this paper was to study the influence of wettability on two-phase flow in 3D granular porous media. The significance of modeling a 3D pore space is that it reveals many aspects of the wettability effect that cannot be captured with the 2D models. The granular medium was generated by the discrete-element method, and care was taken to ensure that the particles had reached their true equilibrium states, before simulating the fluid flow. We utilized a highly resolved CFD-DEM coupling of fluid flow simulation and the mechanics of a granular medium, modeled by the DEM. The VOF method was utilized in the CFD computations, which is known for its efficiency, in order to correctly capture the interface between fluid phases. To obtain accurate results at the pore scale, the immersed boundary method was coupled with the VOF approach. To study the influence of the contact angles on fluid flow in the 3D system, two-phase flow with a range of contact angles was simulated.

Many interesting phenomena was observed in the type of two-phase flow that we studied, including fluid rapture, and dependence of the particle–particle interaction force on the wettability. The simulations indicate that every important characteristic of the system, from those associated with fluid flow, to the mechanics of the granular medium, is influenced by the wettability. Thus, a comprehensive understanding of fluid–solid interactions during two-phase flow in porous media requires a realistic and comprehensive 3D model of the pore space and careful modeling of fluid flow, and taking into account the interaction between the fluids and the solid matrix of the medium. The proposed CFD-DEM approach can identify such micro-scale characteristics in 3D. The proposed framework can be used in 3D systems in order to examine the influence of wettability on the permeability of the medium. Future research can also include other complexities related to both solid and fluid, such as elasticity, morphology, electrostatic properties, and viscosity, and chemical interactions.

Author contribution

MA: Programming, and contributing to the writing of the first draft of the paper. SK, PT, and MS: Conceptualization, supervision of the project, and writing the final draft of the paper. PT and MS funding acquisition.

Data availability

Data will be made available on request.

Declaration of Competing Interest

The authors declare that they have no known competing financial interests or personal relationships that could have appeared to influence the work reported in this paper.

Acknowledgements

Work at both the University of Southern California and the University of Wyoming, was supported by the National Science Foundation grants CBET #2000966 and CBET #2000968.

References

Al-Awadi, H., 2011. Multiphase characteristics of high viscosity oil.
Alhosani, A., Branko Bijeljic, ·, Blunt, M.J., 2021. Pore-Scale Imaging and Analysis of Wettability Order, Trapping and Displacement in Three-Phase Flow in Porous Media with Various Wettabilities 140, 59–84. 10.1007/s11242-021-01595-1.
Aljasmi, A., Sahimi, M., 2021. Speeding-up image-based simulation of two-phase flow in porous media with lattice-Boltzmann method using three-dimensional curvelet transforms. Phys. Fluids 33,. https://doi.org/10.1063/5.0065857 113313.
Al-Raoush, R.I., 2009. Impact of wettability on pore-scale characteristics of residual nonaqueous phase liquids. Environ. Sci. Technol. 43, 4796–4801. https://doi.org/10.1021/ES802566S.
AlRatrout, A., Blunt, M.J., Bijeljic, B., 2018. Wettability in complex porous materials, the mixed-wet state, and its relationship to surface roughness. Proc. Natl. Acad. Sci. USA 115, 8901–8906. https://doi.org/10.1073/PNAS.1803734115/SUPPL_FILE/PNAS.1803734115.SAPP.PDF.
Avlonitis, S.A., Kouroumbas, K., Vlachakis, N., 2003. Energy consumption and membrane replacement cost for seawater RO desalination plants. Desalination 157, 151–158. https://doi.org/10.1016/S0011-9164(03)00395-3.
Baker, M.C., Kong, B., Capecelatro, J., Desjardins, O., Fox, R.O., 2020. Direct comparison of Eulerian-Eulerian and Eulerian-Lagrangian simulations for particle-laden vertical channel flow. AIChE J. 66, e16230.
Bakhshian, S., Rabbani, H.S., Shokri, N., 2021. Physics-Driven Investigation of Wettability Effects on Two-Phase Flow in Natural Porous Media: Recent Advances, New Insights, and Future Perspectives. Transp Porous Media 140, 85–106. https://doi.org/10.1007/S11242-021-01597-Z/FIGURES/10.
Bakhshian, S., Sahimi, M., 2016. Computer simulation of the effect of deformation on the morphology and flow properties of porous media. Phys. Rev. E. https://doi.org/10.1103/PhysRevE.94.042903.
Bartlett, M., Bird, M.R., Howell, J.A., 1995. An experimental study for the development of a qualitative membrane cleaning model. J Memb Sci 105, 147–157. https://doi.org/10.1016/0376-7388(95)00052-E.
Bérard, A., Patience, G.S., Blais, B., 2020. Experimental methods in chemical engineering: Unresolved CFD-DEM. Can J Chem Eng 98, 424–440. https://doi.org/10.1002/CJCE.23686.
Blais, B., Lassaigne, M., Goniva, C., Fradette, L., Bertrand, F., 2016. Development of an unresolved CFD–DEM model for the flow of viscous suspensions and its application to solid–liquid mixing. J Comput Phys 318, 201–221. https://doi.org/10.1016/J.JCP.2016.05.008.
Blunt, M.J., Bijeljic, B., Dong, H., Gharbi, O., Iglauer, S., Mostaghimi, P., Paluszny, A., Pentland, C., 2013. Pore-scale imaging and modelling. Adv Water Resour 51, 197–216. https://doi.org/10.1016/j.advwatres.2012.03.003.
Blunt, M.J., 2017. Multiphase Flow in Permeable Media: A pore-scale perspective.
Bradford, S.A., Abriola, L.M., Leij, F.J., 1997. Wettability effects on two- and three-fluid relative permeabilities. J Contam Hydrol 28, 171–191. https://doi.org/10.1016/S0169-7722(97)00024-7.
Brown, D.W., Duchane, D. v., Heiken, G., Hriscu, V.T., 2012. The Enormous Potential for Hot Dry Rock Geothermal Energy. Mining the Earth's Heat: Hot Dry Rock Geothermal Energy 17–40. 10.1007/978-3-540-68910-2_2.
Cao, G., Li, Q., Wang, R., Wang, C., Duan, X., Ho, S.H., 2020. Simultaneous separation of multiphase emulsion mixture and catalytic degradation of BPA via microalgae residue membranes. Chem. Eng. J. 393,. https://doi.org/10.1016/J.CEJ.2020.124750 124750.
Chiesa, M., Mathiesen, V., Melheim, J.A., Halvorsen, B., 2005. Numerical simulation of particulate flow by the Eulerian-Lagrangian and the Eulerian-Eulerian approach with application to a fluidized bed. Comput Chem Eng 29, 291–304. https://doi.org/10.1016/j.compchemeng.2004.09.002.
Cottin, C., Bodiguel, H., Colin, A., 2010. Drainage in two-dimensional porous media: From capillary fingering to viscous flow. Phys Rev E Stat Nonlin Soft Matter Phys 82. https://doi.org/10.1103/PHYSREVE.82.046315.
Cueto-Felgueroso, L., Juanes, R., 2013. Forecasting long-term gas production from shale. Proceedings of the National Academy of Sciences 110, 19660–19661. 10.1073/pnas.1319578110.
Cueto-Felgueroso, L., Juanes, R., 2008. Nonlocal interface dynamics and pattern formation in gravity-driven unsaturated flow through porous media. Phys Rev Lett 101. https://doi.org/10.1103/PHYSREVLETT.101.244504.
Cundall, P.A., Strack, O.D.L., 1979. A discrete numerical model for granular assemblies. Géotechnique 29, 47–65. https://doi.org/10.1680/geot.1979.29.1.47.
Davydzenka, T., Fagbemi, S., Tahmasebi, P., 2020a. Coupled fine-scale modeling of the wettability effects: Deformation and fracturing. Phys. Fluids 32,. https://doi.org/10.1063/5.0018455 083308.
Davydzenka, T., Fagbemi, S., Tahmasebi, P., 2020b. Wettability control on deformation: Coupled multiphase fluid and granular systems. Phys Rev E 102,. https://doi.org/10.1103/PhysRevE.102.013301 013301.
di Renzo, A., Paolo Di Maio, F., 2005. An improved integral non-linear model for the contact of particles in distinct element simulations. Chem Eng Sci 60, 1303–1312. https://doi.org/10.1016/j.ces.2004.10.004.
Duarte, C.R., Olazar, M., Murata, V. v., Barrozo, M.A.S., 2009. Numerical simulation and experimental study of fluid-particle flows in a spouted bed. Powder Technol 188, 195–205. 10.1016/j.powtec.2008.04.077.
Ebrahimi, M., Willershausen, D., Ashaghi, K.S., Engel, L., Placido, L., Mund, P., Bolduan, P., Czermak, P., 2010. Investigations on the use of different ceramic membranes for efficient oil-field produced water treatment. Desalination 250, 991–996. https://doi.org/10.1016/J.DESAL.2009.09.088.
el Shamy, U., Sizkow, S.F., 2021. Coupled SPH-DEM simulations of liquefaction-induced flow failure. Soil Dyn. Earthq. Eng. 144,. https://doi.org/10.1016/j.soildyn.2021.106683 106683.
Ge, L., Peng, Z., Moreno-Atanasio, R., Doroodchi, E., Evans, G.M., 2020. Three-Dimensional VOF-DEM Model for Simulating Particle Dynamics in the Liquid Slugs of a Vertical Gas-Liquid-Solid Taylor Flow Microreactor. Ind Eng Chem Res 59, 7965–7981. https://doi.org/10.1021/ACS.IECR.0C00108.
Golmohammadi, S., Ding, Y., Kuechler, M., Reuter, D., Schlueter, S., Amro, M., Geistlinger, H., 2021. Impact of Wettability and Gravity on Fluid Displacement and Trapping in Representative 2D Micromodels of Porous Media (2D Sand Analogs). Water Resour Res 57, e2021WR029908. 10.1029/2021WR029908.
Golshan, S., Sotudeh-Gharebagh, R., Zarghami, R., Mostoufi, N., Blais, B., Kuipers, J.A.M., 2020. Review and implementation of CFD-DEM applied to chemical process systems. Chem Eng Sci. https://doi.org/10.1016/j.ces.2020.115646.
Hager, A., Kloss, C., Pirker, S., Goniva, C., 2014. Parallel Resolved Open Source CFD-DEM: Method, Validation and Application: http://dx.doi.org/10.1260/1757-482X.6.1.13 6, 13–28. 10.1260/1757-482X.6.1.13.
Han, Y., Cundall, P.A., 2013. LBM-DEM modeling of fluid-solid interaction in porous media. Int J Numer Anal Methods Geomech 37, 1391–1407.
He, Y., Bayly, A.E., Hassanpour, A., 2018a. Coupling CFD-DEM with dynamic meshing: A new approach for fluid-structure interaction in particle-fluid flows. Powder Technol 325, 620–631. https://doi.org/10.1016/J.POWTEC.2017.11.045.
He, Y., Bayly, A.E., Hassanpour, A., Muller, F., Wu, K., Yang, D., 2018b. A GPU-based coupled SPH-DEM method for particle-fluid flow with free surfaces. Powder Technol 338, 548–562. https://doi.org/10.1016/j.powtec.2018.07.043.
He, L., Liu, Z., Zhao, Y., 2022. An extended unresolved CFD-DEM coupling method for simulation of fluid and non-spherical particles. Particuology 68, 1–12. https://doi.org/10.1016/J.PARTIC.2021.11.001.
Heiba, A.A., Davis, H.T., Scriven, L.E., 1983. Effect of Wettability on Two-Phase Relative Permeabilities and Capillary Pressures. Society of Petroleum Engineers of AIME, (Paper) SPE. 10.2118/12172-MS.
Holtzman, R., 2016. Effects of Pore-Scale Disorder on Fluid Displacement in Partially-Wettable Porous Media. Scientific Reports 2016 6:1 6, 1–10. 10.1038/srep36221.
Issa, R.I., 1986. Solution of the implicitly discretised fluid flow equations by operator-splitting. J Comput Phys 62, 40–65. https://doi.org/10.1016/0021-9991(86)90099-9.
Issakhov, A., Imanberdiyeva, M., 2020. Numerical Study of the Movement of Water Surface of Dam Break Flow by VOF Methods for Various Obstacles. International Journal of Nonlinear Sciences and Numerical Simulation 21, 475–500. https://doi.org/10.1515/IJNSNS-2018-0278/HTML.
Issakhov, A., Zhandaulet, Y., 2020. Numerical Simulation of Dam Break Waves on Movable Beds for Various Forms of the Obstacle by VOF Method. Water Resour. Manag. 34, 2269–2289. https://doi.org/10.1007/s11269-019-02480-9.
Jiang, F., Tsuji, T., Hu, C., 2014. Elucidating the Role of Interfacial Tension for Hydrological Properties of Two-Phase Flow in Natural Sandstone by an Improved Lattice Boltzmann Method. Transp Porous Media 104, 205–229. https://doi.org/10.1007/S11242-014-0329-0.
Kalteh, M., Abbassi, A., Saffar-Avval, M., Harting, J., 2011. Eulerian-Eulerian two-phase numerical simulation of nanofluid laminar forced convection in a microchannel. Int J Heat Fluid Flow 32, 107–116. https://doi.org/10.1016/j.ijheatfluidflow.2010.08.001.

Kloss, C., Goniva, C., Hager, A., Amberger, S., Pirker, S., 2012. Models, algorithms and validation for opensource DEM and CFD-DEM. Progress in Computational Fluid Dynamics 12, 140–152. https://doi.org/10.1504/PCFD.2012.047457.

Kohanpur, A.H., Rahromostaqim, M., Valocchi, A.J., Sahimi, M., 2020. Two-phase flow of CO2-brine in a heterogeneous sandstone: Characterization of the rock and comparison of the lattice-Boltzmann, pore-network, and direct numerical simulation methods. Adv Water Resour 135,. https://doi.org/10.1016/J.ADVWATRES.2019.103469 103469.

Krzysztoforski, J., Jenny, P., Henczka, M., 2018. Porous membrane cleaning using supercritical carbon dioxide. Part 2: Development of mathematical model and CFD simulations. J Supercrit Fluids 136, 1–11. https://doi.org/10.1016/j.supflu.2018.01.028.

Kuang, S., Zhou, M., Yu, A., 2020. CFD-DEM modelling and simulation of pneumatic conveying: A review. Powder Technol 365, 186–207. https://doi.org/10.1016/j.powtec.2019.02.011.

Kuruneru, S.T.W., Marechal, E., Deligant, M., Khelladi, S., Ravelet, F., Saha, S.C., Sauret, E., Gu, Y., 2019. A Comparative Study of Mixed Resolved-Unresolved CFD-DEM and Unresolved CFD-DEM Methods for the Solution of Particle-Laden Liquid Flows. Arch. Comput. Meth. Eng. 26, 1239–1254. https://doi.org/10.1007/S11831-018-9282-3/FIGURES/7.

le Lee, J., Lim, E.W.C., 2017. Comparisons of Eulerian-Eulerian and CFD-DEM simulations of mixing behaviors in bubbling fluidized beds. Powder Technol 318, 193–205. https://doi.org/10.1016/j.powtec.2017.05.050.

Lenormand, R., Touboul, E., Zarcone, C., 1988. Numerical models and experiments on immiscible displacements in porous media. J Fluid Mech 189, 165–187. https://doi.org/10.1017/S0022112088000953.

Li, D., Zhang, J., Zhang, M., Huang, B., Ma, X., Wang, G., 2019. Experimental study on water entry of spheres with different surface wettability. Ocean Eng. 187. https://doi.org/10.1016/J.OCEANENG.2019.106123.

Li, X., Zhao, J., 2018. A unified CFD-DEM approach for modeling of debris flow impacts on flexible barriers. Int J Numer Anal Methods Geomech 42, 1643–1670. https://doi.org/10.1002/nag.2806.

Lin, W., Xiong, S., Liu, Y., He, Y., Chu, S., Liu, S., 2021. Spontaneous imbibition in tight porous media with different wettability: Pore-scale simulation. Phys. Fluids 33,. https://doi.org/10.1063/5.0042606 032013.

Lu, C., Ma, L., Li, Z., Huang, F., Huang, C., Yuan, H., Tang, Z., Guo, J., 2020. A Novel Hydraulic Fracturing Method Based on the Coupled CFD-DEM Numerical Simulation Study. Appl. Sci. 10, 3027. https://doi.org/10.3390/app10093027.

Lungu, M., Siame, J., Mukosha, L., 2021. Comparison of CFD-DEM and TFM approaches for the simulation of the small scale challenge problem 1. Powder Technol 378, 85–103. https://doi.org/10.1016/j.powtec.2020.09.071.

Maggay, I.V., Chang, Y., Venault, A., Dizon, G.V., Wu, C.-J., 2021. Functionalized porous filtration media for gravity-driven filtration: Reviewing a new emerging approach for oil and water emulsions separation. Sep Purif Technol 259,. https://doi.org/10.1016/j.seppur.2020.117983 117983.

Mao, J., Zhao, L., Di, Y., Liu, X., Xu, W., 2020. A resolved CFD–DEM approach for the simulation of landslides and impulse waves. Comput Methods Appl Mech Eng 359,. https://doi.org/10.1016/j.cma.2019.112750 112750.

Meng, Y., Primkulov, B.K., Yang, Z., Kwok, C.Y., Juanes, R., 2020. Jamming transition and emergence of fracturing in wet granular media. Phys Rev Res 2,. https://doi.org/10.1103/PHYSREVRESEARCH.2.022012/FIGURES/4/MEDIUM 022012.

Metz, B., Davidson, O., Coninck, H. de, 2005. Carbon dioxide capture and storage: special report of the intergovernmental panel on climate change.

Nguyen, G.T., Chan, E.L., Tsuji, T., Tanaka, T., Washino, K., 2021a. Resolved CFD–DEM coupling simulation using Volume Penalisation method. Adv. Powder Technol. 32, 225–236. https://doi.org/10.1016/J.APT.2020.12.004.

Nguyen, G.T., Chan, E.L., Tsuji, T., Tanaka, T., Washino, K., 2021b. Interface control for resolved CFD-DEM with capillary interactions. Adv. Powder Technol. 32, 1410–1425.

Nguyen, V.H., Sheppard, A.P., Knackstedt, M.A., Val Pinczewski, W., 2006. The effect of displacement rate on imbibition relative permeability and residual saturation. J Pet Sci Eng 52, 54–70. https://doi.org/10.1016/j.petrol.2006.03.020.

Nhunduru, R.A.E., Jahanbakhsh, A., Shahrokhi, O., Wlodarczyk, K.L., Garcia, S., Maroto-Valer, M.M., 2022. The Impact of Wettability on Dynamic Fluid Connectivity and Flow Transport Kinetics in Porous Media. Water Resour Res 58, e2021WR030729. 10.1029/2021WR030729.

Norouzi, H.R., Zarghami, R., Sotudeh-Gharebagh, R., Mostoufi, N., 2016. Coupled CFD-DEM Modeling: Formulation, Implementation and Application to Multiphase Flows, Coupled CFD-DEM Modeling: Formulation, Implementation and Application to Multiphase Flows. 10.1002/9781119005315.

O'Carroll, D.M., Mumford, K.G., Abriola, L.M., Gerhard, J.I., 2010. Influence of wettability variations on dynamic effects in capillary pressure. Water Resour Res 46. https://doi.org/10.1029/2009WR008712.

Osei-Bonsu, K., Grassia, P., Shokri, N., 2017. Relationship between bulk foam stability, surfactant formulation and oil displacement efficiency in porous media. Fuel 203, 403–410. https://doi.org/10.1016/j.fuel.2017.04.114.

Patel, R.G., Desjardins, O., Kong, B., Capecelatro, J., Fox, R.O., 2017. Verification of Eulerian-Eulerian and Eulerian-Lagrangian simulations for turbulent fluid-particle flows. AIChE J 63, 5396–5412. https://doi.org/10.1002/aic.15949.

Patzek, T.W., Male, F., Marder, M., 2013. Gas production in the Barnett Shale obeys a simple scaling theory. Proc. Natl. Acad. Sci. 110, 19731–19736. https://doi.org/10.1073/pnas.1313380110.

Peng, G., Huang, X., Zhou, L., Zhou, G., Zhou, H., 2020. Solid-liquid two-phase flow and wear analysis in a large-scale centrifugal slurry pump. Eng Fail Anal 114,. https://doi.org/10.1016/j.engfailanal.2020.104602 104602.

Peng, C., Zhan, L., Wu, W., Zhang, B., 2021. A fully resolved SPH-DEM method for heterogeneous suspensions with arbitrary particle shape. Powder Technol 387, 509–526. https://doi.org/10.1016/J.POWTEC.2021.04.044.

Peskin, C.S., 1977. Numerical analysis of blood flow in the heart. J Comput Phys 25, 220–252. https://doi.org/10.1016/0021-9991(77)90100-0.

Pilou, M., Tsangaris, S., Neofytou, P., Housiadas, C., Drossinos, Y., 2011. Inertial Particle Deposition in a 90° Laminar Flow Bend: An Eulerian Fluid Particle Approach. Aerosol Sci. Tech. 45, 1376–1387. https://doi.org/10.1080/02786826.2011.596171.

Pozzetti, G., Peters, B., 2018. A multiscale DEM-VOF method for the simulation of three-phase flows. Int. J. Multiph. Flow 99, 186–204. https://doi.org/10.1016/j.ijmultiphaseflow.2017.10.008.

Rabbani, H.S., Joekar-Niasar, V., Pak, T., Shokri, N., 2017. New insights on the complex dynamics of two-phase flow in porous media under intermediate-wet conditions. Sci. Rep. 7. https://doi.org/10.1038/s41598-017-04545-4.

Rajaei, H., Rajora, A., Haverkort, J.W., 2021. Design of membraneless gas-evolving flow-through porous electrodes. J. Power Sources 491,. https://doi.org/10.1016/J.JPOWSOUR.2020.229364 229364.

Reynolds, C.A., Krevor, S., 2015. Characterizing flow behavior for gas injection: Relative permeability of CO 2 -brine and N 2 -water in heterogeneous rocks. Water Resour. Res. 51, 9464–9489. https://doi.org/10.1002/2015WR018046.

Sahimi, M., 2011. Flow and Transport in Porous Media and Fractured Rock, Flow and Transport in Porous Media and Fractured Rock: From Classical Methods to Modern Approaches: Second Edition. Wiley-VCH Verlag GmbH & Co. KGaA, Weinheim, Germany. 10.1002/9783527636693.

Sahimi, M., 2023. Applications of Percolation Theory. Springer, New York.

Sarkar, D., Sarkar, A., Roy, A., Bhattacharjee, C., 2012. Performance characterization and design evaluation of spinning basket membrane (SBM) module using computational fluid dynamics (CFD). Sep. Purif. Technol. 94, 23–33. https://doi.org/10.1016/J.SEPPUR.2012.03.034.

Shams, M., Singh, K., Bijeljic, B., Blunt, M.J., 2021. Direct numerical simulation of pore-scale trapping events during capillary-dominated two-phase flow in porous media. Transp. Porous Media 138, 443–458. https://doi.org/10.1007/S11242-021-01619-W/FIGURES/10.

Shirgaonkar, A.A., MacIver, M.A., Patankar, N.A., 2009. A new mathematical formulation and fast algorithm for fully resolved simulation of self-propulsion. J. Comput. Phys. 228, 2366–2390. https://doi.org/10.1016/j.jcp.2008.12.006.

Singh, K., Jung, M., Brinkmann, M., Seemann, R., 2019. Capillary-dominated fluid displacement in porous media. Annu. Rev. Fluid Mech. 51, 429–449. https://doi.org/10.1146/ANNUREV-FLUID-010518-040342.

Swain, S., Mohanty, S., 2013. A 3-dimensional Eulerian-Eulerian CFD simulation of a hydrocyclone. Appl. Math. Model. 37, 2921–2932. https://doi.org/10.1016/j.apm.2012.06.007.

Szulczewski, M.L., MacMinn, C.W., Herzog, H.J., Juanes, R., 2012. Lifetime of carbon capture and storage as a climate-change mitigation technology. Proc. Natl. Acad. Sci. USA 109, 5185–5189. https://doi.org/10.1073/PNAS.1115347109/SUPPL_FILE/SAPP.PDF.

Tang, Y., Jiang, Q., Zhou, C., 2018. A Lagrangian-based SPH-DEM model for fluid–solid interaction with free surface flow in two dimensions. Appl. Math. Model. 62, 436–460. https://doi.org/10.1016/j.apm.2018.06.013.

Vångö, M., Pirker, S., Lichtenegger, T., 2018. Unresolved CFD–DEM modeling of multiphase flow in densely packed particle beds. Appl. Math. Model. 56, 501–516. https://doi.org/10.1016/j.apm.2017.12.008.

Wang, Z., Liu, M., 2020. Semi-resolved CFD–DEM for thermal particulate flows with applications to fluidized beds. Int. J. Heat Mass Transf. 159,. https://doi.org/10.1016/J.IJHEATMASSTRANSFER.2020.120150 120150.

Wang, S., Luo, K., Hu, C., Lin, J., Fan, J., 2019a. CFD-DEM simulation of heat transfer in fluidized beds: Model verification, validation, and application. Chem. Eng. Sci. 197, 280–295. https://doi.org/10.1016/j.ces.2018.12.031.

Wang, S., Luo, K., Fan, J., 2020b. CFD-DEM coupled with thermochemical sub-models for biomass gasification: Validation and sensitivity analysis. Chem. Eng. Sci. 217,. https://doi.org/10.1016/J.CES.2020.115550 115550.

Wang, Z., Teng, Y., Liu, M., 2019b. A semi-resolved CFD–DEM approach for particulate flows with kernel based approximation and Hilbert curve based searching strategy. J. Comput. Phys. 384, 151–169. https://doi.org/10.1016/j.jcp.2019.01.017.

Wang, L.K., Wang, M.H., Yaksich, S.M., Granstrom, M.L., 1978. Water treatment with multiphase flow reactor and cationic surfactants. J. Am. Water Works Assoc. 70, 522–528. https://doi.org/10.1002/J.1551-8833.1978.TB04232.X.

Wei, Y., Cejas, C.M., Barrois, R., Dreyfus, R., Durian, D.J., 2014. Morphology of rain water channeling in systematically varied model sandy soils. Phys. Rev. Appl. 2,. https://doi.org/10.1103/PhysRevApplied.2.044004 044004.

Xiong, Q., Madadi-Kandjani, E., Lorenzini, G., 2014. A LBM–DEM solver for fast discrete particle simulation of particle–fluid flows. Contin. Mech. Thermodyn. 26, 907–917. https://doi.org/10.1007/s00161-014-0351-z.

Xu, W.J., Dong, X.Y., Ding, W.T., 2019. Analysis of fluid-particle interaction in granular materials using coupled SPH-DEM method. Powder Technol. 353, 459–472.

Yang, Y., Cai, S., Yao, J., Zhong, J., Zhang, K., Song, W., Zhang, L., Sun, H., Lisitsa, V., 2021. Pore-scale simulation of remaining oil distribution in 3D porous media affected by wettability and capillarity based on volume of fluid method. Int. J. Multiph. Flow 143,. https://doi.org/10.1016/J.IJMULTIPHASEFLOW.2021.103746 103746.

Yang, G.C., Jing, L., Kwok, C.Y., Sobral, Y.D., 2018. A comprehensive study of coupled LBM-DEM with immersed moving boundary. ArXiv. https://doi.org/10.1016/j.compgeo.2019.103100.

Yao, K.M., Habibian, M.T., O'Melia, C.R., 1971. Water and waste water filtration: concepts and applications. Environ. Sci. Technol. 5, 1105–1112. https://doi.org/10.1021/ES60058A005.

Yao, L.M., Xiao, Z.M., Liu, J.B., Zhang, Q., Wang, M., 2020. An optimized CFD-DEM method for fluid-particle coupling dynamics analysis. Int. J. Mech. Sci. 174,. https://doi.org/10.1016/J.IJMECSCI.2020.105503 105503.

Yiotis, A.G., Talon, L., Salin, D., 2013. Blob population dynamics during immiscible two-phase flows in reconstructed porous media. Phys. Rev. E Stat. Nonlin. Soft Matter Phys. 87. https://doi.org/10.1103/PHYSREVE.87.033001.

Yuan, L., Zhou, F., Li, M., Wang, B., Bai, J., 2021. Experimental and numerical investigation on particle diverters transport during hydraulic fracturing. J. Nat. Gas. Sci. Eng. 96. https://doi.org/10.1016/j.jngse.2021.104290.

Zeng, J., Li, H., Zhang, D., 2016. Numerical simulation of proppant transport in hydraulic fracture with the upscaling CFD-DEM method. J. Nat. Gas Sci. Eng. 33, 264–277. https://doi.org/10.1016/j.jngse.2016.05.030.

Zhang, G., Li, M., Gutierrez, M., 2017. Simulation of the transport and placement of multi-sized proppant in hydraulic fractures using a coupled CFD-DEM approach. Adv. Powder Technol. 28, 1704–1718. https://doi.org/10.1016/j.apt.2017.04.008.

Zhang, C., Oostrom, M., Wietsma, T.W., Grate, J.W., Warner, M.G., 2011. Influence of viscous and capillary forces on immiscible fluid displacement: pore-scale experimental study in a water-wet micromodel demonstrating viscous and capillary fingering. Energy Fuel 25, 3493–3505. https://doi.org/10.1021/ef101732k.

Zhang, Y., Ran, Z., Jin, B., Zhang, Y., Zhou, C., Sher, F., 2019. Simulation of particle mixing and separation in multi-component fluidized bed using Eulerian-Eulerian method: a review. Int. J. Chem. React. Eng. 17. https://doi.org/10.1515/ijcre-2019-0064.

Zhao, B., MacMinn, C.W., Juanes, R., 2016. Wettability control on multiphase flow in patterned microfluidics. Proc. Natl. Acad. Sci. 113, 10251–10256. 10.1073/PNAS.1603387113.

Zhang, X., Tahmasebi, P., 2018. Micromechanical evaluation of rock and fluid interactions. Int. J. Greenh. Gas Control 76, 266–277. https://doi.org/10.1016/J.IJGGC.2018.07.018.

Zhang, X., Tahmasebi, P., 2022a. Investigation of particle shape and ambient fluid on sandpiles using a coupled micro-geomechanical model. Powder Technol 117711. https://doi.org/10.1016/j.powtec.2022.117711.

Zhang, X., Tahmasebi, P., 2022b. Coupling irregular particles and fluid: Complex dynamics of granular flows. Comput. Geotech. 143, 104624. https://doi.org/10.1016/j.compgeo.2021.104624.

Zhao, J., Kang, Q., Yao, J., Viswanathan, H., Pawar, R., Zhang, L., Sun, H., 2018. The effect of wettability heterogeneity on relative permeability of two-phase flow in porous media: a lattice Boltzmann study. Water Resour. Res. 54, 1295–1311. https://doi.org/10.1002/2017WR021443.

Zheng, Y., Zhang, W., Tang, B., Ding, J., Zheng, Y., Zhang, Z., 2018. Membrane fouling mechanism of biofilm-membrane bioreactor (BF-MBR): Pore blocking model and membrane cleaning. Bioresour. Technol. 250, 398–405. https://doi.org/10.1016/j.biortech.2017.11.036.

Zhou, C., Wang, W. yuan, Chen, K. xin, Chen, Z. jian, Jung, J., Zhang, S., Chen, Y. min, Bate, B., 2022. Influence of wettability in immiscible displacements with lattice Boltzmann method. J. Zhejiang Univ. A 2022 239 23, 704–720. https://doi.org/10.1631/JZUS.A2200047